Proceedings of the ASME 2017 International Mechanical Engineering Congress and Exposition
IMECE2017
November 3-9, 2017, Tampa, FL, USA

IMECE2017-70954

MULTI-PHYSICS SIMULATION OF COMPLEX FLOW AND PHASE CHANGE INDUCED BY A LOCALIZED LASER IRRADIATION ON A URETHANE-COATED STAINLESS STEEL SUBSTRATE

Yijin Mao, Nazia Afrin, J. K. Chen and Yuwen Zhang[1]
Department of Mechanical and Aerospace Engineering
University of Missouri
Columbia, MO 65211, USA

ABSTRACT

A three-dimensional numerical simulation is conducted for a complex process in a multicomponent-multiphase system, which involves heat and mass transfer in the compressible gaseous phase and chemical reaction during laser irradiation on a urethane paint coated on a stainless steel substrate. A finite volume method (FVM) with a co-located grid mesh that discretizes the entire computational domain is employed to simulate the laser irradiation process. The entire problem is solved within one computational domain that includes two solid regions and one fluid region. To be specific, for the considered solid region, the paint will be decomposed via chemical reaction to gaseous phases then mix into the air and the stainless will involve phase change phenomena, such as melting-solidification and vaporization-condensation, once melting or boiling point is reached. Moreover, the air region is considered as a multi-component phase that has O_2, N_2, CO_2, H_2O, NO_2, binder vapor and stainless vapor. In this multi-physics simulation, the process of melting, vaporization and chemical reaction and the splash of the melted paint and stainless into the air is observed. In the following sections, details on physical models will be given for each key component of the strategy in solving the entire problem. And the last section will show the results and corresponding discussion. This work is done within the framework of the OpenCFD toolbox OpenFOAM [1].

Keywords: Laser irradiation, urethane paint, chemical reaction, compressible flow, melting, vaporization

INTRODUCTION

Due to the unique characteristics of coherency, monochromaticity and collimation, lasers have been widely used in various areas, such as etching and ablation of polyimide [2, 3], ablation of biological tissues [4, 5], and interaction with composite materials [6], to name a few. For many laser applications, scientists and engineers frequently encounter a situation that requires to couple multi-scales and multi-physics in solution of laser-material interaction. For example, laser cutting is one of the most important applications of laser in industry. Thus to accomplish the task in terms of work quality and efficiency, a thorough understanding of the physics that are involved in the laser cutting process is of importance, including thermal transport across the object, change of material themophysical properties, phase change of melting and vaporization, chemical reaction in the material within or nearby the irradiated spot, and discretized particle ejection dynamics in the gaseous phase.

Numerous works on simulation of laser material processing has been published. For example, Mazumder and Steen [7] developed a three-dimensional (3D) heat transfer model for laser material processing with a moving Gaussian heat source using finite difference method. The results showed that some of the absorbed energy is dismissed by radiation and convection from both the top and bottom surfaces of the substrate. Lipperd [8] investigated laser ablation of polymers with designed materials to evaluate the mechanism of ablation. Zhou et al. [9] developed a numerical model to simulate the coupled compressible gas flow and heat transfer in a micro-channel surrounded by solid media. Kim et al. [10] studied the pulsed laser cutting using finite element method, and found that there were some fixed threshold values in the number of laser pulses and power in order to achieve the predetermined amount of material removal and the smoothness of crater shape. As a follow-up work, Kim and Zhang [11] further reported a 3D computational modeling of evaporative laser cutting process. Mahdukar et al. [12] investigated laser paint removal with a continuous wave (CW) laser beam as well as repetitive pulses. The specific energy, a measure of the process efficiency that is defined as the amount of laser energy needed to remove per unit volume of paint prior

[1] Fellow ASME. Corresponding author. Email: zhangyu@missouri.edu

to the onset of substrate damage, was found to be dependent of laser processing parameters. The result also showed that for a CW mode, the specific energy reduced with increase of laser scanning speed, irradiation time, and laser power. Afrin et al [13] conducted a numerical simulation for a complex process in a laser-material system where the effect due to heat/mass transfer, chemical reaction are accounted for. It was found that the chemical reaction mechanism considered is able to capture the paint removal rate in comparison with published experimental data.

The study of simultaneous fluid flow and heat and mass transfer in a coated medium induced by laser heating is scant. Cases of solving problems with material removal and phase change is also rare. The objective of this work is to investigate the effects of laser irradiation on heat transfer and mass destruction of a urethane paint-coated substrate using a 3D numerical simulation. The paint starts melting when the temperature is higher than its melting point and vaporization process will kick in once the boiling point is reached. At the same time, the pigments, one of the main component in paint, will be ejected into the gaseous phase during the vaporization of the liquid paint. Another two possibilities of pigment ejection are surface chemical reaction on the solid paint interacted with gaseous phase and liquid paint splashed into the air. The paint starts to decompose through chemical reaction when the paint's hottest spot reaches its threshold temperature, 560 K. As a result, combustion products CO_2, H_2O and NO_2 are produced and chromium (III) oxide, which is buried (as pigment) in the paint, is ejected as parcels from the paint into the surrounding gaseous domain. The results, including variation of temperature and species concentrations, paint removal by chemical reaction, melting and vaporization, and phase change process of stainless will be analyzed and discussed in detail.

NOMENCLATURE

a	Acceleration (m/s^2)
b	Small value for penalty term
c	Polynomial coefficients
c_p	Specific heat capacity (J/Kg K)
C	Penalty coefficient
d	Diameter of particles (m)
D	Coefficient for penalty term
D_i	Mass diffusion coefficient for species i in the mixture (m^2/s)
D_{ij}	Mass diffusivity coefficient between species *i* and *j*
D^0_{ij}	Mass diffusion coefficient from species i to species j at 298K and 1atm
E	Activation energy (KJ/mol)
$\boldsymbol{F}$	Force (N)
$\boldsymbol{F}^i_p$	Force acting on a single particle in a parcel located in the ith cell
$\boldsymbol{g}$	Gravitational acceleration (m/s^2)
$\mathbf{G}$	Gravity force (N)
h	Enthalpy(J/kg)
H	Specific energy consumption (J/kg)
$\mathbf{I}$	Unit matrix
k	Thermal conductivity (W/m K)
k_c	Chemical reaction rate constant (s^{-1})
K	Arrhenius rate coefficient
m	Mass (kg)
M	Molecular weight (g/mol)
$\mathbf{n}$	Normal vector
N	Number of particles in one parcel
N^i_p	Number of particles in a parcel located in the ith cell
p	Pressure (Pa)
P	Laser power (W); Material properties
q	Heat flux (W/m^2)
r	Radius (m)
R	Universal gas constant (J/Kg K); Beam radius (m)
Re	Reynold number
S	Source term
S_h	Source term in the energy equation
$\boldsymbol{S}_U$	Source term in the momentum equation
t	Time (s)
T	Temperature (K)
$\boldsymbol{U}$	Velocity (m/s)
X_i	Molar fraction of species i

Greeks

α	Volume fraction
α_{ab}	Absorptivity
γ	Ratio of specific heat; Accommodation coefficient for phase change model
λ	Molecular mean free path (m)
μ	Dynamic viscosity(kg/m s)
ρ	Mass density (kg/m^3)
σ	Collision diameter (m); surface tension (N/m)
χ	Surface thermal accommodation coefficient
ψ	Compressibility (s^2/m^2)
ω_i	Mass fraction
Ω	Collision integral

Subscript

c	Chemical reaction; Condensation
b	Binder
abs	Absorptivity
$drag$	Drag force
fm	Free molecular path
i	Index of species
j	Index of species
l	Liquid phase
m	Melting
m-s	Melting and solidification
p	Particle
pg	Pigment
R	Reaction
s	Solid phase
sat	Saturation
v	Vaporization
v-c	Vaporization and condensation
∞	Ambient condition

METHODS AND PHYSICAL MODELS

FLUID PHASES

Since the temperature spans widely in this simulation, from 300K to 3000K, all the fluid phases are considered as a mixture of compressible but immiscible fluids. These fluids contain air, liquid paint, vapor paint, liquid stainless and vapor stainless. The fluid behavior are solved by VOF technique.

$$\frac{\partial \alpha_i}{\partial t} + \nabla \cdot \left(\mathbf{U} \alpha_i \right) = -\frac{\alpha_i \psi_i}{\rho_i} \frac{Dp}{Dt} + \frac{1}{\rho_i} \frac{\dot{m}_i}{\Omega} \tag{1}$$

where α_i, ψ_i and $\dot{m}_i$ represent volumetric fraction, compressibility relevant property and mass change rate of i[th] fluid phase. The mass change rate on the RHS $\dot{m}_i$ could be caused by phase transition and chemical reaction during the process. Such as the chemical reaction of solid paint (or liquid paint) and air will consume oxygen and produce some reactants. The vaporization of liquid paint or liquid stainless (condensation of vapor binder of the paint or vapor stainless) will also attribute this mass change rate. Certain models will be applied to estimate these mass change rates. It is worth mentioning that the phase transition is only about vaporization and condensation in this formalism. The melting and solidification process will be solved directly accordingly once temperature field is obtained. An iterative method is employed to guarantee the accuracy of melting and solidification computation.

PHASE AIR

In consideration of the fact that the mass concentration of each component will change due to phase change and chemical reaction, it is desirable to consider the air as a mixture of multi-components. In this case, we consider the air as a seven-component mixture: O_2, N_2, NO_2, CO_2, H_2O, $vC_3H_7NO_2$ and vStainless. Apparently, Oxygen and Nitrogen are considered because of their dominant role in the air. The three component of NO_2, CO_2 and H_2O are also considered as they are the products of the reaction that is of importance in this case [13]. And the rest two, namely $vC_3H_7NO_2$ and vStainless, represent the vapor of $C_3H_7NO_2$ (binder of the paint) and stainless. The mass concentration of each species will be computed by solving the following equation,

$$\frac{\partial \rho \omega_i}{\partial t} + \nabla \cdot (\rho \omega_i \mathbf{U}) = \rho \nabla \cdot \left[D_i \nabla \omega_i \right] + S_i \tag{2}$$

The mass diffusivity of the i^{th} specie (D_i) in Eq. (2) can be determined using the Maxwell-Stefan mass transport model [14] that considers the multi-species system as a special binary system,

$$D_i = \frac{1 - X_i}{\sum_{j, j \neq i} (X_i / D_{ij})} \tag{3}$$

where X_i denotes the molar fraction of specie i, and D_{ij} are the mass diffusivity between specie i and j that is temperature and pressure dependent [15]:

$$D_{ij} = D_{ij}^0 \frac{T^{\frac{3}{2}}}{p} \tag{4}$$

where D_{ij}^0 is the mass diffusivity from specie i to j at 300 K and 1 atm. It can be determined by combining Chapman-Enskog theory and the method introduced by Bird et al. [14] as follows:

$$D_{ij}^0 = \frac{1.858 \times 10^{-3} T_0^{3/2} \sqrt{1/M_i + 1/M_j}}{p_0 \sigma_{ij}^2 \Omega} \tag{5}$$

where T_0 and p_0 are room temperature and atmosphere pressure, σ_{ij} is the average collision diameter of species i and j, and Ω is a collision integral which is tabulated in [16]. The source term will be attributed to chemical reactions and phase changes.

SOLID PHASE

The paint, as considered as a homogenous mixture of binder ($C_3H_7NO_2$) and pigment (Cr_2O_3), will be solved through a pure heat conduction equation as,

$$\frac{\partial}{\partial t} \left(\rho c_p T \right) = \nabla \cdot \left(k \nabla T \right) \tag{6}$$

where ρ and c_p and k represent density, specific heat and thermal conductivity, respectively. These properties are a mole weighting of all components. For each component, these properties are all considered as either constant or temperature dependent to meet various users need.

Chemical reaction

In order to consider the surface receding due to the chemical reaction, the most commonly accepted model of estimating chemical reaction rate, Arrhenius equation, is adopted to compute mass loss during the paint decomposition process. The reactant rate of binder ($C_3H_7NO_2$) that is defined as the mass of binder reacted per unit area per unit time, is computed by [9]:

$$\dot{m} = K(T) C_{o_2} \tag{7}$$

where $\dot{m}$ has unit of kg/m^2/s and C is oxygen's concentration which has unit of kg/m^3. The Arrhenius equation [17] can be expressed as:

$$K(T) = K_0' \, \mathrm{e}^{-E/RT} \tag{8}$$

where the coefficient K_0' is estimated as:

$$K_0' = \left(RT / 2\pi M_{O_2} \right)^{1/2} \tag{9}$$

where E is activation energy of the binder, and M_{O2} is molar weight of oxygen.

The surface receding velocity can be calculated as,

$$\frac{\dot{m}}{\rho_b} = \frac{K(T) C_{o_2}}{\rho_b} = \frac{K_0' \, \mathrm{e}^{-E/RT} C_{o_2}}{\rho_b} = \left(RT / 2\pi M_{O_2} \right)^{1/2} \mathrm{e}^{-E/RT} \frac{C_{o_2}}{\rho_b} \tag{10}$$

After known mass consumed rate, the total energy absorbed by the chemical reaction is

$$q = \dot{m} \left| \nabla \alpha \right| H_R \tag{11}$$

where gradient of α indicate the interface between solid (or liquid) paint to the air and H_R is energy consumption per unit mass of binder.

Injection Model

Since the paint is a two-component mixture, which consist of binder and pigment that have two different boiling points, it is true that those pigments will be released into the gaseous phase once the solid paint is in reaction or the liquid paint is in vaporization. This phenomenon is realized by arranging many hidden injectors in the computational meshes that is occupied

with solid or liquid paint. The amount that ejected into the air is computed as

$$m_p = m_b \omega_p / \omega_b \tag{12}$$

where ω is mass fraction of corresponding component in the paint. This expression is practical, since the mass change rate of the binder can be found from the chemical reaction or vaporization-condensation model. Then the number of the particle in a single parcel can be simply determined by volume conversation through assuming all the particles are spherical.

Solid particles

Once the solid parcels are released into the gaseous phases, three behaviors have to be captured, namely, the motion and trap of parcel if it moved into liquid phases, and rebound if it collides with solid paint or stainless. At the end of this subsection, the heat transfer model between solid particle and surrounding air is also given.

In the aspect of parcels' motion, these parcels' trajectory can be described using the Newton's 2nd law,

$$m\mathbf{a} = \mathbf{G} + \mathbf{F}_{drag} \tag{13}$$

where m and $\mathbf{a}$ are mass and acceleration of a particle. The right hand side of Eq. (13) accounts for gravity $\mathbf{G}$ and the drag force $\mathbf{F}_{\text{drag}}$ due to the velocity difference from the gaseous phase. The drag force is estimated in consideration of particle's sub-micro size [18] as follows [19]:

$$\mathbf{F}_{drag} = \left[\frac{3}{4} m \mu_c \left(\frac{24}{C_c} \right) \Big/ \rho_p d_p^2 \right] \left(\mathbf{U} - \mathbf{U}_p \right) \tag{14}$$

where μ_c is molecular viscosity of the fluid, $\mathbf{U}_\text{p}$ is the velocity of the particle, and C_c is the Cunningham correction to Stokes' drag law [18]:

$$C_c = 1 + \frac{2\lambda}{d_p} \left(1.257 + 0.4 e^{-\frac{1.1 d_p}{2\lambda}} \right) \tag{15}$$

in which λ is the molecular mean free path. The gravitational force is calculated by:

$$\mathbf{G} = m\mathbf{g} \left(1 - \frac{\rho}{\rho_p} \right) \tag{16}$$

The trap behavior of parcels will be treated by simply adjusting the velocity of the particle in the following mean:

$$\mathbf{U}^{\mathbf{new}} = \mathbf{U}^{\mathbf{old}} - 2\mathbf{sign}\left(-\mathbf{U}^{\mathbf{old}} \cdot \mathbf{n} \right) \left(\mathbf{U}^{\mathbf{old}} \cdot \mathbf{n} \right) \mathbf{n} \tag{17}$$

where $\mathbf{n}$ means the normal direction of interface between two different phases. The last behavior, parcel collision with solid region, is considered as a pure elastic collision, therefore, the velocity after collision can be expressed as:

$$\mathbf{U}^{\mathbf{new}} = \mathbf{U}^{\mathbf{old}} - 2\mathbf{sign}\left(\mathbf{U}^{\mathbf{old}} \cdot \mathbf{n} \right) \left(\mathbf{U}^{\mathbf{old}} \cdot \mathbf{n} \right) \mathbf{n} \tag{18}$$

On the heat transfer between solid particle and surrounding air, it is done by pre-assuming its relaxation time is shorter than the simulation's time step. With this assumption, the work to be done is only about estimating heat transfer coefficient between the solid particles and surrounding phases. Since the pigment particle has size in the scale of sub-micro, the mean of computing heat transfer coefficient has to consider the effect due to the mean free path of air molecules. With this in mind, the following expression is adopted [20] for the heat transfer coefficient,

$$h_{fm} = \frac{\chi}{2} \frac{P_\infty}{T_\infty} \sqrt{\frac{RT_\infty}{2\pi}} \frac{\gamma + 1}{\gamma - 1} \tag{19}$$

where χ is surface thermal accommodation coefficient, P_∞ and T_∞ are 1atm and room temperature, R is universal gas constant, γ is ratio of specific heats.

The metal, which serves as the substrate of the solid region, is also solved as a pure heat conduction problem. Similar to the paint region, the thermal properties are also considered as temperature dependent, which are expressed as polynomial functions:

$$P = \sum_{i=0}^{7} c_i T^i \tag{20}$$

where P represent any material properties, such as density, specific heat and thermal conductivity.

Momentum equation should also be solved for the melted region of the stainless. A penalty method, which consider this effect by adding a large value for the solid phase of the computational domain, is applied.

$$\begin{aligned} &\frac{\partial \rho \mathbf{U}}{\partial t} + \nabla \cdot (\rho \mathbf{U}) \mathbf{U} + D\mathbf{U} = -\nabla p - \rho \mathbf{g} \\ &\quad + \nabla \cdot \left[\mu \nabla \mathbf{U} - \frac{2\mu}{3} trace(\nabla \mathbf{U}) \mathbf{I} \right] + \mathbf{S}_{\sigma_n} + \mathbf{S}_{\sigma_t} + \mathbf{S}_\mathbf{u} \end{aligned} \tag{21}$$

where D is a large number for the region with small volume of liquid. This value will vanish for the pure liquid region, since the mathematical expression is

$$D = C \frac{(1-\alpha)^2}{\alpha^3 + b} \tag{22}$$

The fourth term, the RHS of the momentum equation, is about surface tension effect [21]. As can be seen, this force is considered as proportional to the local curvature of the interface as following:

$$\mathbf{S}_{\sigma_n} = \sum_i \sum_{i<j} \sigma_{i,j} K_{i,j} \left(\alpha_i \nabla \alpha_j - \alpha_j \nabla \alpha_i \right) \tag{23}$$

The fifth term is about tangential component of surface tension, or called Marangoni stress. It is related to the temperature gradient by the expression as following [22]:

$$\mathbf{S}_{\sigma_t} = \frac{d\sigma}{dT} \left(\nabla T - \mathbf{n} \left(\mathbf{n} \cdot \nabla T \right) \right) |\nabla \alpha| \tag{24}$$

The last term is about the momentum exchange between particle and surrounded fluids. It is estimated through momentum conversation between these two phases [23].

$$\mathbf{S}_\mathbf{u} = -\sum_p N_p \mathbf{F}_p \tag{25}$$

where $\mathbf{F}_\text{p}$ is representing the force acting on the particle per volume, N_p is number of particles in one single parcel.

Melting and Solidification

As mentioned previously, the melting and solidification process is iteratively solved along with the energy equation. Since the phase change occurs in this simulation work, a source term that introduces the latent heat and sensitive heat have to be accounted for. The energy equation that is written in temperature form can be derived from the one in enthalpy form and rewritten as,

$$\frac{\partial(\rho cT)}{\partial t}+\nabla(\rho c\mathbf{U}T)=\nabla\cdot(k\nabla T)+\left[T_m\left(\frac{\partial(\rho c)}{\partial t}+\nabla(\rho c\mathbf{U})\right)-L_m\left(\frac{\partial(\rho_l\alpha_l)}{\partial t}+\nabla\cdot(\rho_l\alpha_l\mathbf{U})\right)\right] \quad (26)$$

Once the temperature is known, the volumetric fraction of liquid will be estimated by [24],

$$\alpha_l=\left(erf\left[\frac{4(T-T_m)}{T_l-T_s}\right]+1\right)\Big/2 \quad (27)$$

The obtained α_l will be substituted into the equation (26), and the volumetric fraction of liquid will be estimated respectively. This iteration process will not terminate until both temperature and volumetric fraction are converged.

Vaporization and Condensation

Similar to the melting and solidification, the energy equation that account for source terms on the latent and sensitive heat due to vaporization and condensation can be written as,

$$\frac{\partial(\rho cT)}{\partial t}+\nabla(\rho c\mathbf{U}T)=\nabla\cdot(k\nabla T)+\left[T_{sat}\left(\frac{\partial(\rho c)}{\partial t}+\nabla(\rho c\mathbf{U})\right)-L_v\frac{\dot{m}}{\Omega}\right] \quad (28)$$

To compute the phase change rate, Lee's model [25], which considered the phase change rate as proportional to multiplication of the super-heat or sub-cool and the volumetric fraction of liquid or vapor phase, is employed. The following mathematical expressions give the condensation and vaporization rate respectively:

$$\frac{\dot{m}_l}{\Omega}=\gamma_v\rho_v\alpha_v\frac{T_{sat}-T}{T_{sat}},T<T_{sat} \quad (29)$$

$$\frac{\dot{m}_v}{\Omega}=\gamma_c\rho_l\alpha_l\frac{T-T_{sat}}{T_{sat}},T>T_{sat} \quad (30)$$

where both γ_v and γ_c are accommodation coefficient specified by user. An appropriate pair of these empirical values will lead interface temperature to the saturated temperature once the phase change occur.

In addition, since the laser is considered as an external source, the ultimate expression of energy equation could be expressed as,

$$\frac{\partial(\rho cT)}{\partial t}+\nabla(\rho c\mathbf{U}T)=\nabla\cdot(k\nabla T)+S_{m-s}+S_{v-c}+S_{chem}+S_{laser} \quad (31)$$

where the subscript "*m-s*" represents melting and solidification, "*v-c*" indicates "vaporization and condensation". Currently, the mathematical expression of this laser source is

$$S_{laser}=\int_S qdS\Big/\int_\Omega qdV \quad (32)$$

where q is

$$q=\alpha_{abs}\frac{P}{\pi R^2}e^{-r^2/R^2} \quad (33)$$

where α_{abs}, P, and R represent absorptivity coefficient, laser power and beam radius. It is worth pointing out that the laser source heat should be considered as a boundary condition, however, as stated in [26], treating this as a body source is accurate enough once the depth of thermal diffusion for the laser pulse duration is large compared to the optical attenuation depth. It is also should be pointed out that the energy irradiated on solid phase is considered as a net absorbed energy.

RESULTS AND DISCUSSION

COORDINATION NUMBER AND PACKING FRACTION

Figure 1 illustrates the physical and geometric model of the problem under consideration. A solid (paint + stainless steel) with a size of l×w×h (length×width×height) in the x-, z- and y-directions is placed at the bottom of the entire simulation domain that has a size of L×W×H (length×width×height). The dimensions used in the simulation are 250×250×200 mm3 for the gaseous domain and 30×30×1.35 mm3 for the solid domain. The thickness is 0.150 mm for paint and the rest 1.2 mm for stainless steel (AISI 304L). In other words, the thickness of the paint is 150 μm.

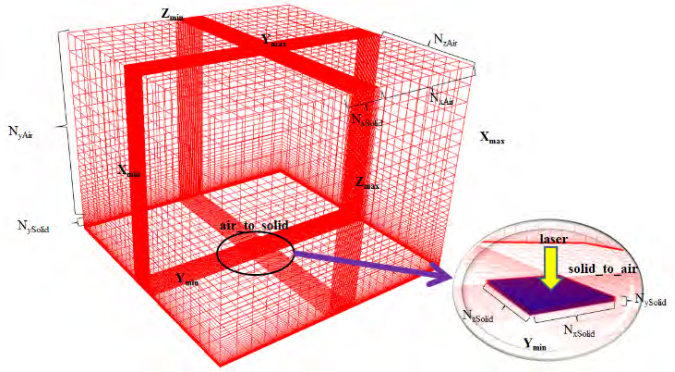

Figure 1 Illustration of computational domain

Table 1 Material properties of the solids

	Cr_2O_3 Pigment	$C_3H_7NO_2$ Binder	Stainless Steel AISI 304L
Conductivity (W/m K)	32.94	0.4	$7.9318+0.023051T$ $-6.4166\times10^{-6}T^2$
Heat capacity (J/kg K)	781	1755	$426.7+0.17T$ $-5.2\times10^{-5}T^2$
Density (Kg/m^3)	5210	1424	7900
Melting Point (K)	-	323	1670
Solidus temperature (K)		320	1669
Liquidus temperature (K)		326	1671
Melting Latent Heat (K/Kg)		1×10^5	2.73×10^5
Saturation temperature (K)		455	2999
Vaporization Latent Heat		1×10^6	7.6×10^6
Heat of Chemical Reaction (J/Kg)		6.28×10^6	
Activation Energy (J/mole)		45×10^3	
Chemical Reaction Threshold temperature (K)		560	

The paint is a homogenous mixture of binder ($C_3H_7NO_2$) and pigment (Cr_2O_3), which takes 40% of binder and 60% of pigment, respectively. The thermal properties of paint and stainless applied are given in the following tables.

The Absorptivity of paint is considered as constant of 0.7, while it is treated as a polynomial function of temperature for the stainless.

$$\alpha_{abs}=\begin{cases}0.363-2.16\times10^{-4}T+1.92\times10^{-7}T^2-3.73\times10^{-12}T^3 & T\in[300,1670]\\ 0.536 & T\in[1670,\infty]\end{cases} \quad (34)$$

The Table 1 shows the material properties of the solid phases [27]. The diffusion properties for the gaseous phase are given in the Table 2.

Table 2 Mass diffusion coefficient of each pair of components in the air ($\times 10^{-5} m^2/s$)

	O_2	N_2	CO_2	H_2O	NO_2	$vC_3H_7NO_2$	vStainless
O_2	/	2.037	1.509	2.769	1.559	1.0	1.0
N_2	2.037	/	1.499	2.69	1.556	1.0	1.0
CO_2	1.509	1.499	/	2.079	1.109	1.0	1.0
H_2O	2.769	2.69	2.079	/	2.177	1.0	1.0
NO_2	1.559	1.556	1.109	2.177	/	1.0	1.0
$vC_3H_7NO_2$	1.0	1.0	1.0	1.0	1.0	/	1.0
vStainless	1.0	1.0	1.0	1.0	1.0	1.0	/

The thermal properties of gaseous components are shown in the following Table 3.

Table 3 Thermal properties of each component in the air

	O_2	*N_2*	*CO_2*	*H_2O*	*NO_2*	*$vC_3H_7NO_2$*	*vStainless*
c_p (kJ/kg K)	0.918	0.807	0.846	1.86	1.04	/	/
μ ($\times 10^{-5}$ Pa s)	2.06	1.78	1.51	1.23	1.33	/	/

The surface tension (N/m) of each phase pair are given in the Table 4.

Table 4 Surface tension between each phase in consideration

	lstainless	lpaint	air	paint	stainless
lstainless	/	0	1.98	0	0
lpaint	0	/	0	0	0
air	1.98	0	/	0	0
paint	0	0	0	/	0
stainless	0	0	0	0	/

The coefficient used for Marangoni force is given in the following Table 5.

Table 5 The coefficient of tangential surface tension. (N/m/K)

	lstainless	lpaint	air
lstainless	/	-0.43×10^{-5}	-0.43×10^{-5}
lpaint	-0.43×10^{-5}	/	0
air	-0.43×10^{-5}	0	/

Five cases with different laser source that has power of 15KW, 12.5KW, 10KW, 7.5KW and 5KW and same beam radius of 2.0 mm are used to demonstrate the capability of solving the complicated heat and mass transfer phenomena induced by a localized laser irradiation on a urethane-coated stainless substrate.

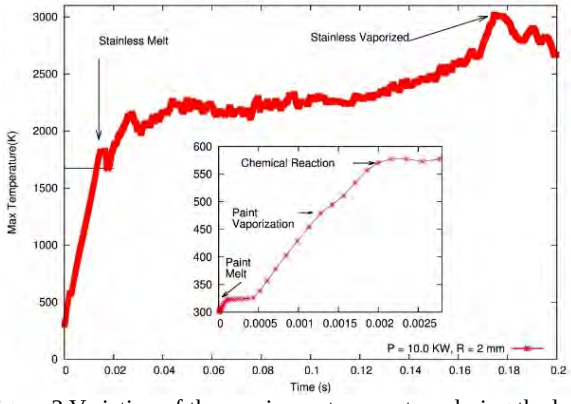

Figure 2 Variation of the maximum temperature during the laser irradiation for the case with laser power of 10 KW.

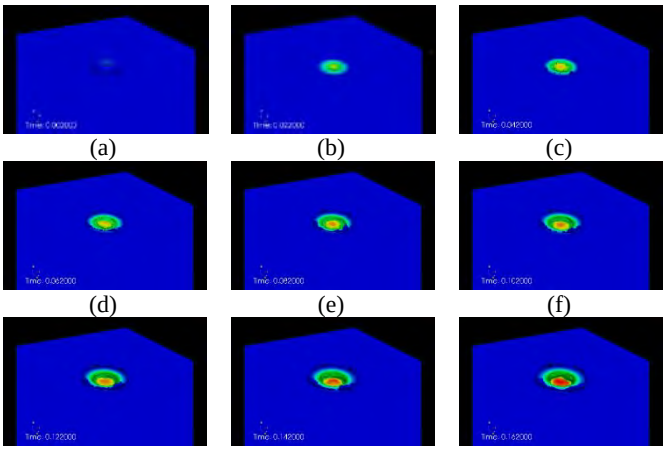

Figure 3 Solid and liquid phase during the laser irradiation Power =10 KW, R = 2 mm, $I_{max} = 7.96\times10^4$ W/cm^2 (Colored by temperature)

Figure 2 shows the maximum temperature variation along with time during the laser irradiation. The laser power applied is 10.0 KW while its beam radius is 2 mm. As can be seen, this figure shows some important turning points. From its subplot, a nearly flat zone start at time of 0.2 ms when the temperature is close to 323K which is the melting point of the paint. This flat zone ends at time of 0.42 ms when the paint at the central domain are completely melted. In the following period, another flat zone which indicates vaporization of liquid paint is not clearly observed. The main reason for this phenomena is that the Marangoni stress smears the liquid paint to the side of the crater created by the laser when the melting phenomena is in processing. In other words, the vaporization of liquid paint is mainly carried out at the side of laser irradiation spot. It is also seen that an obvious drop appears in the immediate following period, when the tempertature reaches to 560K. This is due to the chemical reaction. At time of 0.02s, it is found another drop comes out along the cuve at temperature of 1822K which is higher than the melting point of stainless. At time of 0.182s,

vaporization of liquid stainless occurs. In its following period, the temperature falls down due to energy absorption by latent heat.

Figure 3 shows the melting process of paint and stainless during laser irradiation at various times.In Figure 3 (a), the liquid paint is smeared by Marangoni stress which pushes the liquid to the surrouding area where the temperature is relatively lower. In Figure 3 (b), the liquid paint is gone due to vaporization, however, stainless which exposed to the laser source starts melting at the center of the heated spot. In Figure 3 (c), the melting process continues and liquid stainless is also pushed to the surrounding area due to Marangoni stress. In the Figure 3 (c) ~ (i), as can be seen, the liquid accumulates, meanwhile, a clear crater is created by the laser.

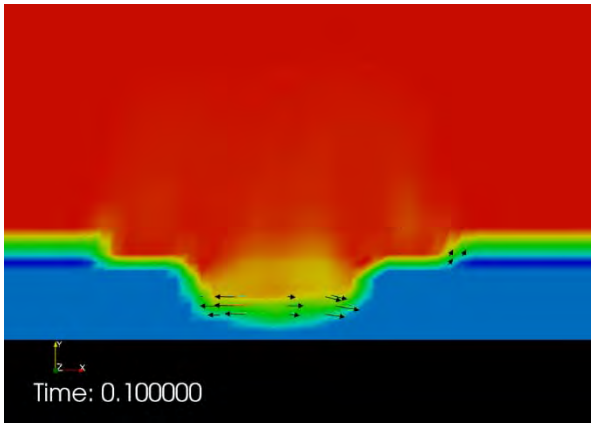

Figure 4 Marangoni force push on the interface between liquid and gas, the arrows indicate the direction of Marangoni force

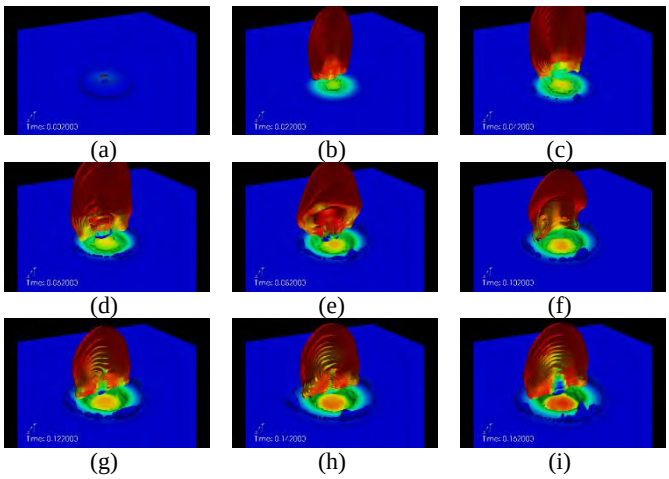

Figure 5 Contour of vapor paint and stainless

In order to have a better understanding on how Marangoni force pushes the liquid, Figure 4 shows all existing phases in the compuational domain and Marangoni forces. As indicated by the arrows. Marangoni force driving the fluid to the surrounding area where temperature is relatively lower.

Figure 5 shows the growing process of the mixture vapor of paint and stainless by ploting its contour. As shown in Figure 5 (a), almost no vapor exist at the very beginning. However, at time of 0.022 s, vapor of paint appears. It should be pointed out that this vapor region must be pure paint, since the temperature during the period from 0.2 ms to 162 ms is still lower than saturation temperature of liquid stainless according to the Figure 2. From Figure 5 (c) to (f), it is shown that the vapor region is decreasing, this is caused by mass diffusion in the air. However, Figure 5 (g) to (i) shows that the vapor region grows again. This is due to continuing vaporization of liquid paint from the surrounding area.

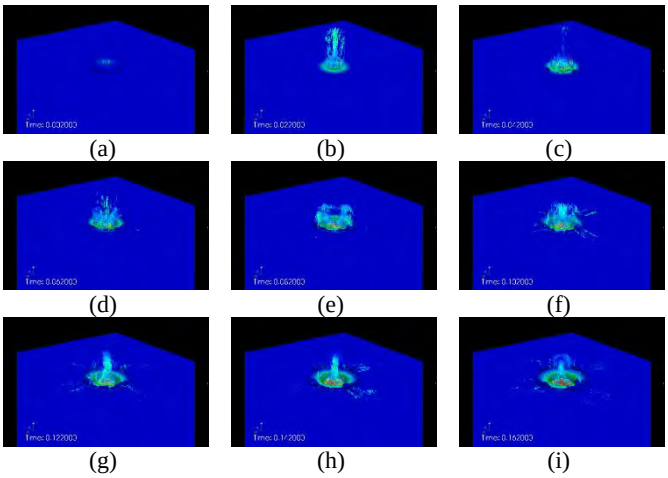

Figure 6 Ejection of pigment particles

Figure 6 gives the parcels' ejection during the paint removal process. Each little arrow represents a parcel (a group of particles which has same properties), and the direction is its moving velocity. In Figure 6 (a), a few of parcels are released from the vaporized paint. In the Figure 6 (b), a large number of parcels are ejecting into the air due to local natural convection which is clearly caused by larger temperature difference between heated substrate and surrounding air. As can be seen, the parcels are still moving upward in the Figure 6 (c). However, some parcels at the top are falling down, as shown in Figure 6 (d). This could happen as the drag force exerted on the parcels cannot hold its gravity. In Figure 6 (e) and (f), as shown, most parcels are pushed to the surrounding area after the falling parcels hits the paint. It could be explained according to the locally disturbed momentum due to motion of the falling parcel. In fact, the velocity which are supposed to be directing upward now turns upside down because of the drag force acting on the parcel. Moreover, the velocity in the region right adjacent to the liquid paint or stainless is parallel to the interface between gaseous phase and liqud phase, and directing to the lower temperarture region due to Marangoni force. Due to these two factors, the majority of the parcels are moving toward the surrounding area, as shown in Figure 6 (g) ~ (i).

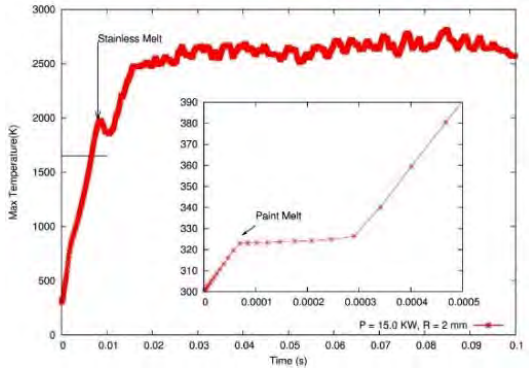

(a)

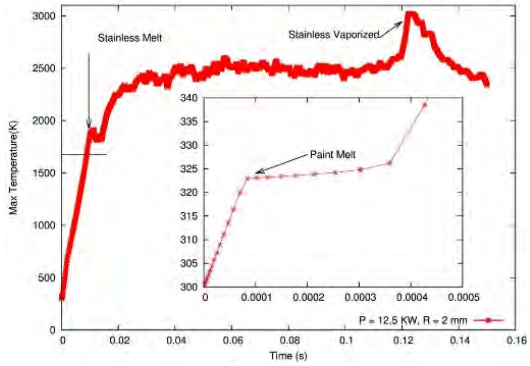

(b)

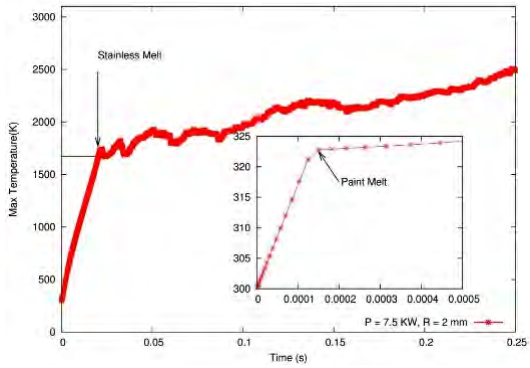

(c)

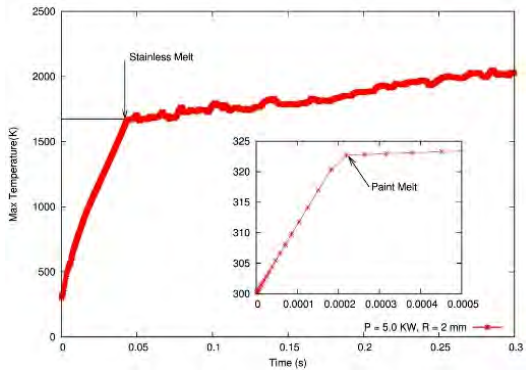

(d)

Figure 7 Variation of the maximum temperature during the laser irradiation for the cases with laser powers of (a) 15.0 KW, (b) 12.5 KW, (c) 7.5 KW, and (d) 5.0 KW.

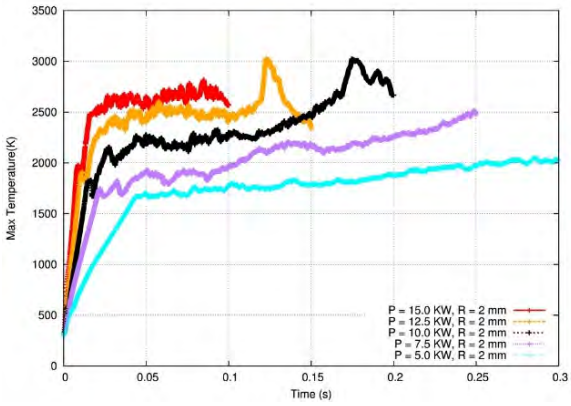

Figure 8 comparison of five cases with different laser power

In order to have a better understanding on how the laser power affects the entire heating process. Another four cases, which includes two cases have higher power while the other two have relatively lower laser power, are simulated and the results are presented in the following sections.

Figure 7 shows time variation of the maximum temperature in the compuational domain during the heating process. It is found that all cases show a similar turning point where melting, chemical reaction and vaporization occur. The Figure 7 (a) shows the case with laser power of 15.0 KW, the total simulation time is 0.1s. It is observed that the vaporization does not occur when the simulation ends. While for the case shown in Figure 7 (b) which has laser power of 12.5 KW, vaporization occurs at time of around 0.13s. To the case with laser power of 7.5 KW and 5.0 KW, the maximum temperatures only reach up to 2500K and 2000K when the simulations end at 0.25s and 0. 30s.

Figure 8 has combined all five curves on temperature variation together. As shown, only two cases has reached the stage of the vaporization of the liquid stainless.

CONCLUSION

In this work, a multi-physics solver which is capable to solve a multiphase system that induced by a localized laser irradiation on a urethane-coated stainless steel substrate therefore involve chemical reaction, heat and mass transfer is developed based on OpenFOAM-2.3.0.

The gases are considered as multicomponent system with certain compressibility. The paint and stainless is able to account for both melting-solidification and vaporization-condensation phenomena. The chemical reaction on the surface of paint and between liquid paint and air are both considered. Five cases with different laser powers, 15.0 KW, 12.5 KW, 10.0 KW, 7.5 KW and 5.0 KW, but same laser beam of 2 mm are performed for 0.1s, 0.15s, 0.20s, 0.25s and 0.30s respectively. Different stages of heating process, melting of solid paint, vaporization of liquid paint, chemical reaction of paint, melting of solid stainless and vaporization of liquid stainless, can be captured by this solver. Smearing of the liquid paint and stainless, due to Marangon forces, is also observed. Vapor of paint and stainless are also seen for two out of the five cases. The parcels that released from paint

after chemical reaction or vaporization, are ejected into the surrounding area. The motion of those ejected particles (pigments) are also capatured in this simulation.

REFERENCES

[1] Weller, H. G., Tabor, G., Jasak, H., Fureby, C., "A Tensorial Approach to Computational Continuum Mechanics Using Object-Oriented Techniques," *Computers in physics*, 1998; **12**(6): pp. 620-631.

[2] Brannon, J. H., Lankard, J. R. , Baise, A. I. , Burns, F., Kaufman, J. , "Excimer Laser Etching of Polyimide," *Journal of Applied Physics*, 1985; **5**(58): pp. 2036-2043.

[3] Sobehart, J. R., "Polyimide Ablation Using Intense Laser Beams," *Journal of Applied Physics*, 1993; **4**(74): pp. 2830-2833.

[4] Lane, R. J., Wynne, J. J., Gernonemus, R.G., "Ultraviolet Laser Ablation of Skin: Healing Studies and a Thermal Model," *Lasers in surgery and medicine*, 1986; **6**: pp. 504-513.

[5] Lecartentier, G. L., Motamedi, M., McMath, L. P., Rasregar, S., Welch, A. J., "Continuous Wave Laser Ablation of Tissue: Analysis of Thermal and Mechanical Events," *IEEE Transactions on Biomedical Engineering*, 1993; **40**: pp. 188-200.

[6] Chen, J. K., Perea, A., Allahdadi, F. A., "A Study of Laser/Composite Material Interactions," *Composite Science and Technology*, 1995; **54**: pp. 35-44.

[7] Mazumder, J., Steen, W. M., "Heat Transfer Model for Cw Laser Material Processing," *Journal of Applied Physics*, 1979; **51**: pp. 941-947.

[8] Lipperd, T., "Laser Application in Polymers," *Advances in Polymer Science*, 2004; **168**: pp. 51-246.

[9] Zhou, J. H., Zhang, Y. W., Chen, J. K. , "Numerical Simulation of Compressible Gas Flow and Heat Transfer in a Microchannel Surrounded by Solid Media," *Int Journal of Heat and Fluid Flow*, 2007: pp. 1484-1491.

[10] Kim, M. J., Zhang, J., "Finite Element Analysis of Evaporative Cutting with a Moving High Energy Pulsed Laser," *Applied Mathematical Modeling*, 2001; **25**: pp. 203-220.

[11] Kim, M. J., "Three Dimentional Finite Element Analysis of Evaporative Laser Cutting," *Applied Mathematical Modeling*, 2005; **29**: pp. 938-954.

[12] Madhukar, Y. K., Mullick, S. , Shukla, D. K. , Kumar, S. , Nath, A.K. , "Effect of Laser Operating Mode in Paint Removal with a Fiber Laser," *Applied Surface Science*, 2013; **264**: pp. 892-901.

[13] Nazia, A., Mao, Y., Zhang, Y., Chen, J.K., Ritter, R., Lampson, A., Stohs, J., "Multicomponent Gas-Particle Flow and Heat/Mass Transfer Induced by a Localized Laser Irradiation on a Urethane-Coated Stainless Steel Substrate," *Frontiers in Heat and Mass Transfer (FHMT)*, 2016; **7**(1).

[14] Bird, R. B., Stewart, W. E., Lightfoot, E. N. Transport Phenomena. New York: John Wiley & Sons; 1960.

[15] Faghri, A., Zhang, Y., Howell, J. R. Advanced Heat and Mass Transfer: Global Digital Press; 2010.

[16] Hirschfelder, J. O., Curtiss, C.F., Bird, R. B. Molecular Theory of Gases and Liquids: Wiley; 1964.

[17] Laidler, K. J., "The Development of the Arrhenius Equation," *Journal of Chemical Education*, 1984; **61**(6): p. 494.

[18] Ounis, H., Ahmadi, G., McLaughlin, J. B., "Brownian Diffusion of Submicrometer Particles in the Viscous Sublayer," *Journal of Colloid and Interface Science*, 1991; **143**(1): pp. 266-277.

[19] Haider, A., Levenspiel, O., "Drag Coefficient and Terminal Velocity of Spherical and Nonspherical Particles," *Powder Technology*, 1989; **58**(1): pp. 63-70.

[20] Hiers, R., "Rarefaction Effects in Small Particle Combustion," *Journal of Thermophysics and Heat Transfer*, 1997; **11**(2): pp. 232-238.

[21] Brackbill, J., Kothe, D. B., Zemach, C., "A Continuum Method for Modeling Surface Tension," *Journal of computational physics*, 1992; **100**(2): pp. 335-354.

[22] Saldi, Z. S., "Marangoni Driven Free Surface Flows in Liquid Weld Pools," *Delft University of Technology, The Netherlands*, 2012.

[23] Cai, J., Yuan, Z., Zhao, X., "Study on Two-Way Coupling of Gas–Solid Two-Phase Flow of Cylindrical Particles," *Powder Technology*, 2016; **300**: pp. 136-145.

[24] Rösler, F., Brüggemann, D., "Shell-and-Tube Type Latent Heat Thermal Energy Storage: Numerical Analysis and Comparison with Experiments," *Heat Mass Transfer*, 2011; **47**(8): pp. 1027-1033.

[25] Sun, D., Xu, J., Chen, Q., "Modeling of the Evaporation and Condensation Phase-Change Problems with Fluent," *Numerical Heat Transfer, Part B: Fundamentals*, 2014; **66**(4): pp. 326-342.

[26] Bechtel, J. H., "Heating of Solid Targets with Laser Pulses," *Journal of Applied Physics*, 1975; **46**(4): pp. 1585-1593.

[27] Weast, R. C., Astle, M. J., Beyer, W. H. CRC Handbook of Chemistry and Physics: CRC press Boca Raton, FL; 1988.